Incremental capacity analysis of lithium-ion second-life batteries from electric vehicles under cycling ageing

Elisa Braco, Idoia San Martín, Pablo Sanchis, Alfredo Ursúa
Department of Electrical, Electronic and Communication Engineering
Institute of Smart Cities
Public University of Navarre
Pamplona, Spain
elisa.braco@unavarra.es

***Abstract*— Nowadays, the reuse of batteries from electric vehicles is considered a promising solution to benefit from their remaining energy and extend their lifespan. Yet, the economic viability of these second-life batteries is still uncertain, and the optimization of testing at their reconfiguration stage and during their lifetime is the key to ensure their success. This paper aims to assess Incremental Capacity Analysis technique in Nissan Leaf modules during their second-life use, in order to evaluate both its potential as an State of Health estimator and as a tool to identify underlying degradation mechanisms. Despite the different internal state and ageing rates observed between the tested modules, ICA is found to be consistent at similar SOH levels. The influence of ageing, current and temperature on ICA is evaluated through an accelerated cycling test. Results show that ICA is a promising alternative to estimate SOH during second life even at currents up to C/2 and testing temperatures of 45 °C. However, testing by accelerated currents and temperatures is not recommended for the identification of degradation mechanisms.**

Keywords—Incremental Capacity Analysis, cycling ageing, second-life batteries, electric vehicles

I. INTRODUCTION

Automotive transition towards electric vehicles (EV) is already a fact, prompted by environmental problems related to traditional ICE vehicles, government actions and citizen awareness. In 2020, the number of EVs surpassed 10 million units worldwide, with an annual increase of 40 % despite the global pandemic situation. This expansion had a direct impact on the demand for Li-ion batteries, which reached 160 GWh in 2020 [1].

During their usage in EVs, Li-ion batteries suffer from degradation related to both operation and rest, in the so-called cycle and calendar aging. This degradation leads to capacity and power fade in the batteries, which may compromise their compliance with EV requirements. Therefore, automotive standards set a 20 % loss of capacity as the withdrawal point for batteries from EVs. Given their impact on the price of EVs, batteries reuse emerges as a cost-reduction alternative to recycling. Stationary applications such as energy storage on residential photovoltaic installations, with operating profiles less demanding than EVs and in which power and energy density are not so crucial, are promising scenarios of reuse. The potential of these second-life batteries (SLB) from EV batteries is such that their global market is expected to reach 26 GWh by 2025 [2].

However, the commercial success of SLB is yet to be guaranteed because it depends on their technical and economic viability. Over the last few years, the operation [3], [4] and durability [5] of SL modules from EVs has been experimentally assessed. Moreover, the performance of reused EV battery packs has been tested in different applications with high power requirements, such as frequency regulation [6], or high energy demand, namely residential energy time shifting and demand side management scenarios [7]. Nevertheless, the economic viability of SLB is still uncertain nowadays. The cost of SLB is determined up to 30 % by the repurposing process [8]. In this step, characterization of reused batteries is key, in order not only to guarantee SL application requirements, but also to decrease the impact of dispersion between reconfigured modules, which can be up to four times greater than in their new homologues [3]. Conventional characterization methods consist of several hours of testing, with a sequence of charge and discharge cycles to measure capacity, and EIS or current pulses to obtain the internal impedance. Despite the accuracy of these methods, the time and equipment necessary to carry them out are a major barrier to reducing reconfiguration costs.

In recent years, Incremental Capacity Analysis (ICA) has emerged as an alternative to characterization methods. The great potential of this technique lies in its dual role. On the one hand, ICA is a non-destructive method to determine the degradation mechanisms of the cells [9], [10]. On the other hand, it is also a promising method to estimate the State of Health (SOH) of Li-ion batteries at cell [11] and battery pack level [12], with accurate results at acceptable computational cost. However, ICA requires low current testing to achieve representative results [13] or applying complex filtering methods to decrease the measurement noise [14].

Despite its possibilities, ICA has barely been studied in retired EV batteries during their SL. As SOH estimator, this technique was applied to 6 NMC cells from BMWi3 EV and 6 LMO cells from Nissan Leaf EV aged under calendar testing, being the results validated in 3 real battery packs [12]. The influence of cycling aging was suggested in this contribution as a possible cause of the differences observed in EVs. In [15], 24 LMO modules retired from Renault Kangoo EV were tested, concluding that SOH estimation was influenced by the C-Rate of ICA measurement. From its part, [16] tested 6 SL LFP modules also at their retirement point, proved that IC tracking could be a fast-screening method for SLB.

Considering the research gap in this field, this work aims to analyse ICA in retired EV batteries during their SL lifetime. Moreover, the possibility of accelerating the IC testing

procedure will also be considered, given its potential regarding the economic viability of SLB. The contribution is based on experimental results, which include extended cycling ageing tests. The paper is organized as follows: Section II focuses on the experimental setup, with SL modules and experimental procedure description, Section III shows and discusses the results obtained, focusing on ageing, influence of current and temperature. Finally, Section IV gathers the main conclusions of this contribution.

II. Experimental Setup

A. Module description

The Li-ion battery modules under study in this paper were specially designed for automotive purposes, in particular for the Nissan Leaf EV. Each module is composed of four pouch-type cells of manganese oxide/graphite (LMO/C), associated in two parallel-connected pairs in series (2s2p). As Fig. 1 shows, three external terminals are available: positive (R), middle point (W) and negative (B), in such a way that 2p cells are the smallest testing unit. The nominal capacity of the modules is 66 Ah, and their maximum, minimum and nominal voltages are 8.3 V, 5 V, and 7.5 V, respectively.

B. Experimental procedure

The experimental procedure described in this section is carried out at 2p cell level, between R and W terminals. To ease reading, the 2p cells will be hereafter named as cell.

a) Incremental Capacity Analysis

In this contribution, ICA is obtained from constant current charges test files with a sampling interval of 1 second. Each charge is split into 200 sections of equal time, considering this number as a compromise between measurement noise and IC detection. For each section (n to n+1), voltage and capacity change are obtained, computing the incremental capacity (IC) as the differentiation of the battery charging capacity (Q) against the voltage (V), according to (1).

$$IC = (dQ/dV)_n = (Q_n - Q_{n+1}) / (V_n - V_{n+1}) \quad (1)$$

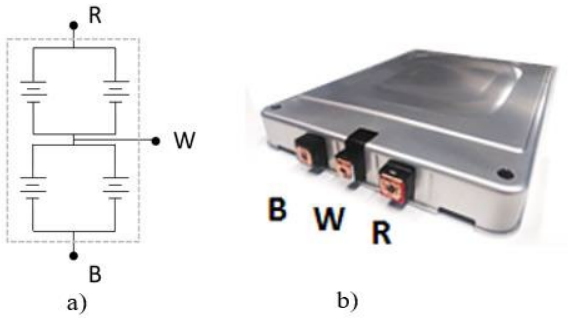

Fig. 1. a) Internal module scheme and b) Nissan Leaf EV module.

Measurement noise in the IC curve is mitigated through a moving average filtering of 12 points. This solution is found to be the best compromise between accuracy and simplicity. Peak and valley identification is performed on the filtered IC curves using 'findpeaks' function in Matlab. The minimum distance between peaks and valleys is set to 30 points, and the minimum height to 5 points.

b) Reference Performance Tests (RPT)

To characterize capacity, internal resistance and IC curve of the cells, RPT are carried out periodically every four weeks. For this purpose, the ambient temperature is controlled at 25 °C±1 ºC. The RPT procedure starts with a 24-hour rest at the test temperature, so that the cells reach thermal equilibrium. The RPT sequence of testing is then carried out as follows:

- Capacity test. Three full cycles between cell voltage limits at C/3. The charging procedure is Constant Current (CC) until maximum cell voltage followed by a Constant Voltage (CV) phase until a cut-off current of C/30 is reached. Discharges are CC until minimum cell voltage. The capacity discharged in the third cycle is considered as the actual capacity of the cell.
- DC internal resistance pulse test. After a full charge, cells are discharged until the specified State of Charge (SOC) level with a CC pulse. Then, a 1-hour rest is set, so that cells reach thermodynamic equilibrium, followed by a CC discharge pulse until the next SOC level. Both charge and discharge C-Rate are C/2. DC internal resistance (DCIR) is computed from voltage and current measurements at the end of the rest period and after 10 seconds of discharge pulse. The SOC intervals are 20 %, starting at 90 % SOC.
- IC curve. After a 1-hour rest, cells are fully charged at C/30, in order to determine their IC curve.

c) Cycling ageing tests

The cycling ageing tests are carried out at a controlled ambient temperature of 45 °C±1 ºC. After a 24-hour rest, cells are CC discharged at C/3 until their minimum voltage, and then charged at the same rate until a SOC of 75 %. Then, a cycling sequence with CCCV charges and CC discharges at 0.7 C is applied with a 50 % of Depth of Discharge (DOD). Both SOC and DOD are computed from the actual capacity of the cell. Every 100 equivalent full cycles, capacity and DCIR measurement tests are carried out at the same temperature.

C. Test bench

The test bench consists of a battery tester and a climatic chamber. The battery tester stands 5 V and 50 A on each channel, accurate to within ±0.1 % of full scale, while the climatic chamber allows a temperature range from -30 °C to +180 °C with measurement precision of ±0.5 ºC.

III. Results and Discussion

A. ICA in SLB

Two SL cells are tested according to the RPT described in Section III, being the main results presented in Table I. This point will be hereafter considered as SL Beginning of Life (SL-BOL). As it can be seen, capacity results show great differences, despite being both samples SL cells. The SOH of Cell 1 is 91.1 %, while in Cell 2 this value decreases to 71.3 %. Internal resistance measurements also vary, being it 13 % greater in Cell 2. These differences could be due to their FL history and subsequent degradation rates. While Cell 2 is consistent with the automotive retirement standards regarding capacity, Cell 1 could have been a replacement never used which would have degraded under calendar aging effects. The differences observed evidence the heterogeneity of reused batteries at their SL-BOL.

Fig.2 shows the IC curve of Cell 1 and Cell 2 at their SL-BOL. The IC is plotted in the Y axis, while voltage is shown in the X axis. Four peaks can be identified in Cell 1, while Cell 2 only shows two. This is consistent with other IC studies of

cells with similar SOH and chemistry [12]. As explained before, the amplitude and shape of the peaks is related to the electrochemical processes of the electrodes, giving valuable information about the underlying degradation mechanisms.

Table I shows the IC and voltage position of each feature of the curve from Fig.2. As it can be seen, the main electrochemical reactions occur at voltages greater than the nominal cell value (3.75 V). Hence, the operation of cells at high SOC would entail greater degradation than at low voltages [17]. In general, IC curve of Cell 2 is shifted to higher voltages, which can be related to the increase of its internal resistance [10]. From the four original peaks of Cell 1, Peak 2 (P2) and Peak 4 (P4) disappear in Cell 2, while the IC of Peak 1 (P1) and Peak 3 (P3) increase 42.9 % and 24.5 % respectively. The decrease of IC peaks has traditionally been related to loss of active material (LAM) [10], [17], which combined with loss of lithium inventory (LLI) are responsible

TABLE I. RPT RESULTS AT SL-BOL

RPT result	Cell	
	1	*2*
Capacity (Ah)	60.18	47.07
DCIR (mΩ)	1.64	1.86
Peak 1 - IC (Ah·V-1); V (V)	100.85; 3.745	144.11; 3.795
Peak 2 - IC (Ah·V-1); V (V)	183.65; 3.925	-
Peak 3 - IC (Ah·V-1); V (V)	172.58; 4.012	214.82; 4.024
Peak 4 - IC (Ah·V-1); V (V)	243.10; 4.079	-
Valley 1 - IC (Ah·V-1); V (V)	65.91; 3.801	66.93; 3.885
Valley 2 - IC (Ah·V-1); V (V)	156.22; 3.976	-
Valley 3 - IC (Ah·V-1); V (V)	78.72; 4.055	-

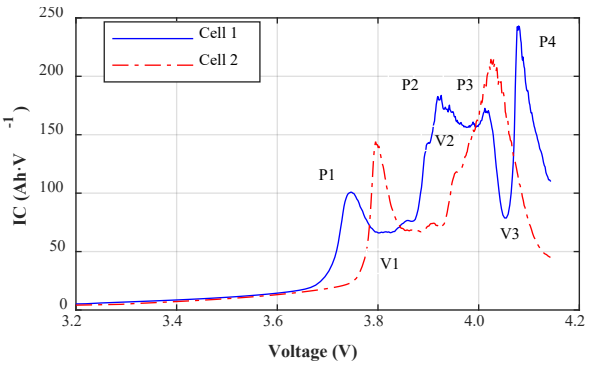

Fig. 2. Voltage vs. IC in Cell 1 (blue) and Cell 2 (red) at SL-BOL.

of peak fade [10], [17]. On the other hand, two of the three original valleys disappear in Cell 2, which is consistent with the aforementioned vanishing of P2 and P4 in Cell 1. Valley 1 (V1) does not change in IC but in voltage, which could imply that the underlying reaction in the electrodes remains unchanged with ageing. The overall differences observed in both IC curves are consistent with the capacity and DCIR measurements, as Cell 2 was found to be much more degraded.

This first approach to ICA in SLB shows that this technique also allows to detect heterogeneity of reused batteries at their BOL. Several questions arise, such as how IC curves evolve with ageing in both cells, or whether they are consistent at equivalent SOH levels. Hence, the next step of this contribution analyses the behaviour of IC curves with ageing.

B. Influence of SOH in ICA of SLB

In order to determine the evolution of IC curves at different SOH, Cell 1 and Cell 2 are aged according to the accelerated cycling test described in Section III.

Fig.3 shows the evolution of capacity and DCIR measurements in the RPTs during the ageing test, referred to their initial value at SL-BOL, which is gathered in Table I. The Equivalent Full Cycles (EFC) performed by the cells during the test are plotted in the X axis. As the figure shows, even though capacity fades linearly with EFC in both cells, the slope is 3.5 times greater in Cell 2, leading to a higher degradation rate under similar cycling. After 1181 EFC, capacity from Cell 2 reaches a SOH level of 23.8 %. On the other hand, the SOH of Cell 1 reaches 68.1 % after 1505 EFC, which is similar to the SL-BOL state of Cell 2. Considering DCIR increase, both cells show a quadratic correlation with EFC, but the degradation rate is much higher in Cell 2. At the end of the test, the DCIR of Cell 2 has increased 232 % from its SL-BOL value, while DCIR of Cell 1 only 36 %. The different degradation rates observed in both cells could be due to their FL usage, which would have been much more aggressive in Cell 2.

Fig. 4 shows the IC curves of Cell 1 (a) and Cell 2 (d) measured during their cycling ageing test. For each curve, the corresponding SOH level measured is stated and coloured differently. SOH in Cell 1 varies from 91 % to 68 %, while in Cell 2 it goes from 71 % to 24 %. As the figure plots, there is a change of shape in the IC curve of Cell 1, with the fade and disappearance of P2 and V1 at SOH values below 79 % and of P4 and V3 below 71 %. The resulting shape is consistent

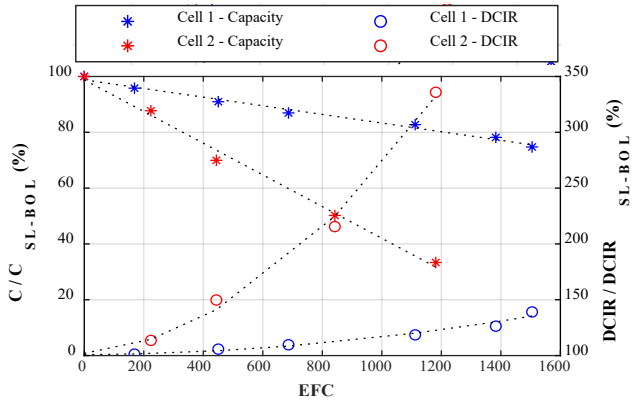

Fig. 3. Capacity and DCIR measured in RPTs of Cell 1 (blue) and Cell 2 (red) during cycling ageing test related to their SL-BOL.

with the IC curve of Cell 2 at its SL-BOL, which was measured at similar SOH. To ease graph tracking, Fig. 4 also plots the evolution of peaks and valleys in IC magnitude for Cell 1 (b) and Cell 2 (e) related to their value at SL-BOL. As it can be seen, IC in peak 4 (P4@IC) experiences the greatest fade, until 59 % of its initial, while P2@IC fades 15 % before vanishing. From its part, P1@IC increases up to 21 % and remains constant and the other points do not change more than 5 % during the test. On the other hand, in Cell 2, P1@IC and P3@IC fade up to 28 % and 38 % of their initial value, respectively. The decrease of peaks is traditionally related to LAM [10], while the sequence observed, with the fade and

vanish of P4 and later decrease of P3 could also be due to LLI in the anode [10]. Both LAM and LLI are considered to be mainly caused by Mn dissolution in LMO cells [18]. Finally, the voltage position of peaks and valleys is shown in Cell 1 (c) and Cell 2 (f). As it can be seen, there is a general increase of all voltages with SOH, which would be related to the resistance increase measured during the test [10]. The voltage in valley 2 (V2@V) is an exception to this trend. This relation is more evident at high aging states, where the increase in voltage is quadratic with the value at SL-BOL, being this trend similar to the one observed in DCIR.

Considering ICA as a tool for SOH estimation, there is a linear correlation between some indicators and SOH. The best results in Cell 1 are P4@V and V1@V, which R-square of linear regression are 0.995 and 0.993, respectively. In Cell 2, the best results are obtained in P1@IC and V1@IC, with R-square of 0.998 and 0.994. However, to track the whole SL lifetime, the indicator should appear in both cells, and its trend with SOH should be consistent. Thereby, the voltage in V1 shows the best result, with an overall R-square of the linear fitting of 0.879. This finding is consistent with previous analysis of similar cells [12].

The results shown were measured according to the RPT procedure described in Section III. At their SL-BOL, the IC test took almost 1170 minutes in Cell 1, and 930 minutes in Cell 2. Given the necessity of reducing testing time, the following sections will analyse the potential of acceleration factors such as current and temperature increase.

C. Influence of C-Rate in ICA of SLB

As a first acceleration factor, this section will investigate the influence of C-Rate in ICA of SLB. For this purpose, IC curve is determined at C/3 and C/2 from corresponding charges of the RPT measurement described in Section II. As different rates are aimed to be compared, the influence of polarization resistance is considered [9], [13]. To do so, the IC curve is compensated with the corresponding DCIR for every SOC level considered in the RPT.

Fig. 5 shows IC curve of Cell 2 at its SL-BOL as representative behaviour. As it can be observed, if current increases, the general shape of the curve is maintained, with the greatest difference obtained in P3. At C/3, P3@IC fades 18.2 % with respect to C/30, while at C/2 it decreases up to 24.8 %. On the contrary, V1@IC and V1@V are found to vary less than 1 % with C-Rate.

Given the differences observed between indicators, the influence of C-Rate in the evolution of IC and voltage measurements is analysed during the ageing test. The error in peak and valley identification is defined as the difference between the corresponding current (C/3 or C/2) with respect to C/30, related to their value at C/30. Fig. 6 shows the error results in absolute value during the whole ageing test, with the corresponding SOH plotted in the X axis. In view of the previous analysis, only the most relevant indicators are shown. Hence, V1 voltage (V1@V) is kept for its SOH estimation potential, while IC in P1 (P1@IC), P3 (P3@IC), and P4 (P4@IC) are selected to identify degradation mechanism.

As Fig.6 shows, voltage measurement is much more precise than IC. While V1 tracking shows a maximum error of 1.1 % during all the ageing tests, IC measurement leads to errors between 10.1 % and 64.3 % at C/3 and 15.3 % and 60.1 % at C/2. It should be highlighted that some points cannot be identified if C-Rate increases. In Cell 1, P4 vanishes in the last RPT at both rates, while P1, P3 and V1 disappear at C/2 in the last RPT of Cell 2. The differences in behaviour observed at high C-rates could be due to inhomogeneous lithium

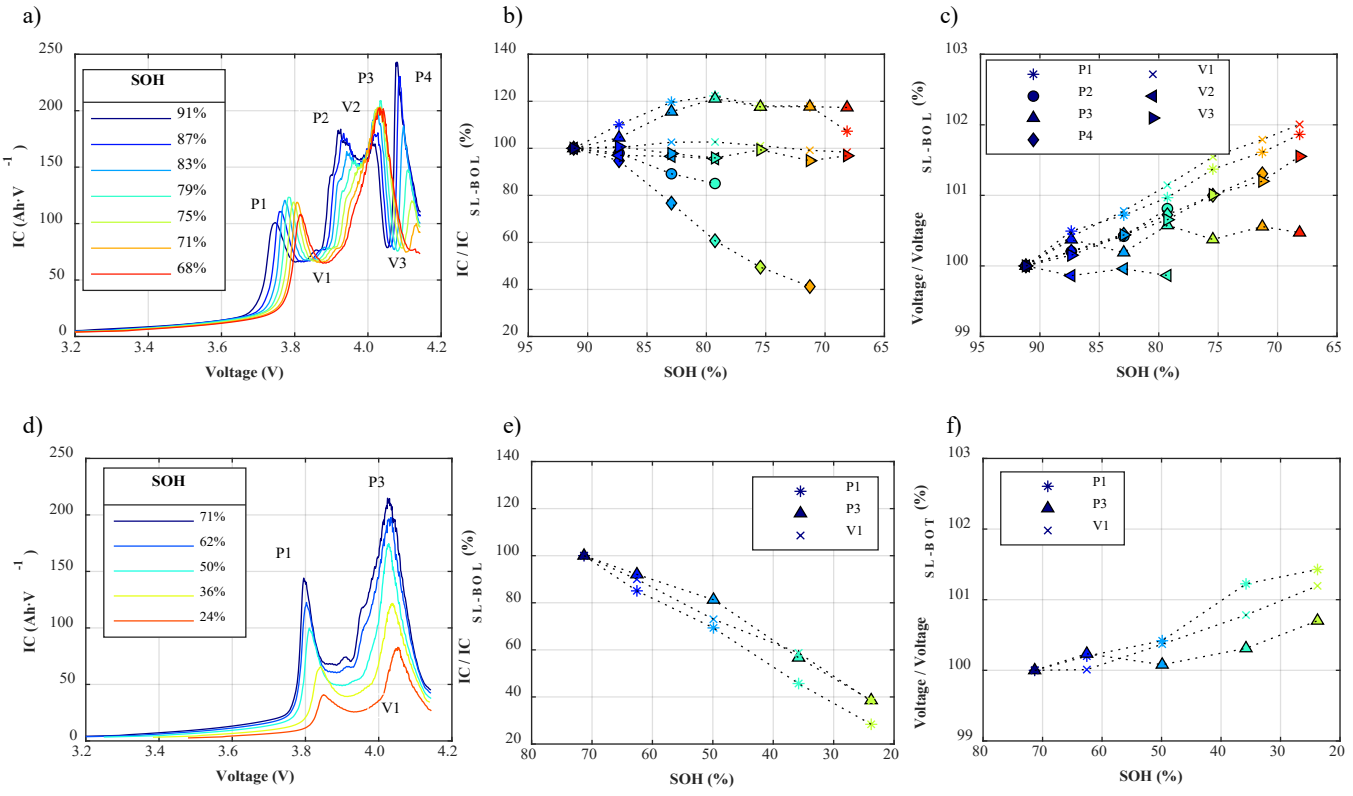

Fig. 4 a) Voltage vs. IC curve, b) SOH vs. IC magnitude and c) SOH vs. voltage magnitudes related to the SL-BOLmeasurements in Cell 1 and d) Voltage vs. IC curve, e) SOH vs. IC magnitude and f) SOH vs. voltage magnitudes related to the SL-BOL of Cell 2.

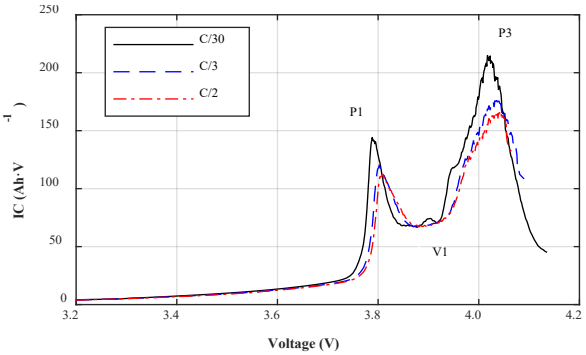

Fig. 5. IC curve at C/30, C/3 and C/2 at SL-BOL in a) Cell 2.

distribution [19]. This effect is a consequence of the increase in concentration gradients in the electrodes and the reduction of the relaxation time of the phases to equalize, both promoted by high charge and discharge rates.

Ageing is found to negatively affect IC estimation at C/3 and C/2. This is especially relevant in P3@IC, where error increases as both cells age. On the contrary, only the error in V1@V is completely independent of SOH in both samples. Regarding testing times, they were reduced to 165 and 150 minutes in Cell 1 and 130 and 110 minutes in Cell 2 at C/3 and C/2 respectively at their SL-BOL. Compared to the 1170 minutes in Cell 1 and 930 minutes in Cell 2 at C/30, this time reduction states the interests of increasing C-Rate to accelerate IC testing.

D. Influence of temperature in ICA of SLB

This section analyses the influence of test temperature in the ICA of SLB. For this purpose, from the accelerated cycling test described in Section III, two temperatures are compared: 25 °C and 45 °C. The analysis is held at both C/3 and C/2.

Fig.7 shows the IC plot at SL-BOL of Cell 2. As it can be seen, the increase in temperature does not influence curve shape. Considering IC magnitude, peaks are slightly enlarged, as for instance P1@IC is 4.5 % greater at 45 °C while valleys remain almost invariable. The capacity measured at 45 °C is 3.1 % greater than at 25 °C, what would explain the differences observed.

Given the interest of studying the evolution during the whole lifetime of the cells, the measurement error between temperatures for a given C-Rate is computed as the difference between 45 °C and 25 °C results, related to the 25 °C measurement. Fig. 8 shows the absolute value of the errors of the most relevant indicators previously discussed for Cell 1 and Cell 2, with the SOH measured at the corresponding RPT plotted in the X axis. As Fig.8 shows, temperature increase adversely affects both IC and voltage. This is especially noticeable with ageing, and as it can be seen, IC error in Cell 2 can be up to 38.8 %, while in Cell 1 it is lower than 24.1 %. Moreover, peak detection is also adversely affected with temperature, as P3 is missed at C/3 in the last RPT, and P4 is only tracked at SL-BOL in Cell 1 at C/3. Voltage measurement is much more precise as temperature increases, with errors lower than 1.5 % at C/2 and 1.3 % at C/3.

IV. Conclusions

This contribution assesses ICA on SL modules from Nissan Leaf EVs under different aging states. Given the potential of this technique, the aim is to evaluate its possibilities as SOH estimator and as a tool to identify degradation mechanisms. To do so, IC curves were obtained at two temperatures and three currents during an accelerated cycling test in two 2p cells from different SL modules. Thereby, the influence of three factors on ICA in SL cells has been analysed: ageing, current and temperature.

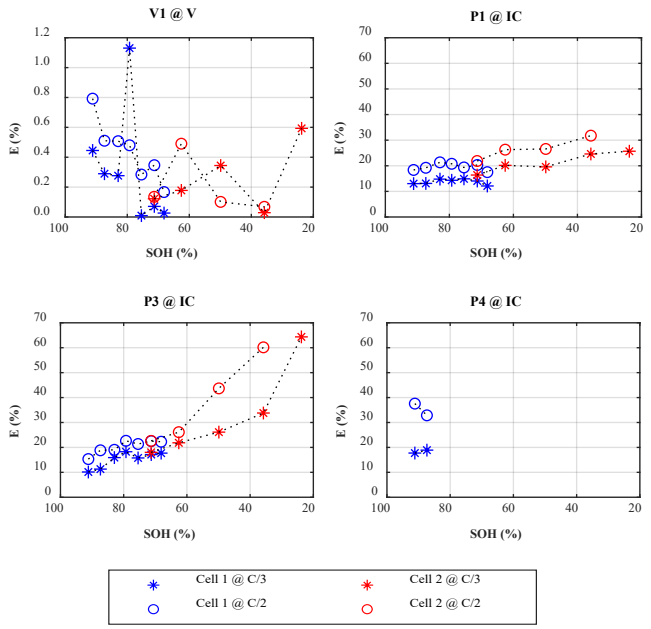

Fig. 6. IC and voltage measurement error of the most relevant indicators at C/3 and C/2 related to C/30 during the cycling ageing test.

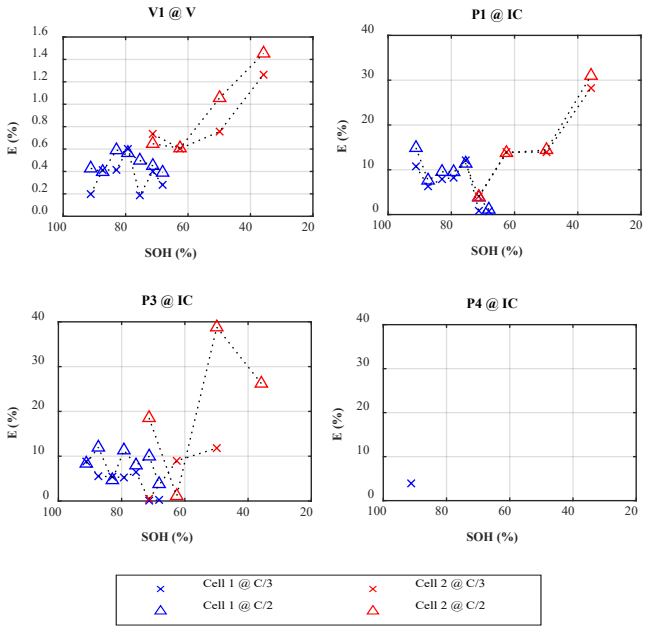

Fig. 7. IC and voltage measurement error of the most relevant indicators at 45 °C related to 25 °C at C/3 and C/2 during the cycling ageing. test.

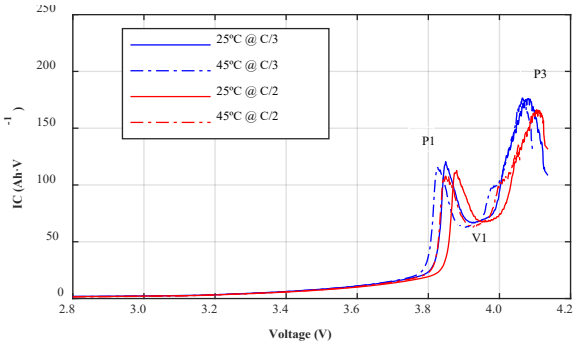

Fig. 8. IC curve of Cell 2 at C/2 and C/3 at 25 °C and 45 °C at SL-BOL.

The initial state of the cells, as well as and their degradation rate during cycling ageing were different, which confirmed the inhomogeneity of characteristics and ageing tends of reused cells from EVs. However, IC curves were found to be similar at close SOH levels, suggesting that this technique is suitable for SLB. Peak behaviour in both cells was consistent with typical degradation mechanisms of Li-on batteries, such as LAM and LLI. Moreover, resistance increase was observed from the voltage shift of the curves during ageing. Regarding SOH estimation, voltage in valley 1 was stated to be the best indicator, as it appeared in both cells with a consistent trend between them. The SOH range tested covered from 92 % to 24 %, assessing thereby a wide SL range.

Considering current as an acceleration factor of ICA, voltage errors compared to the lowest testing C-rate were under 1.2 %, which encourages the use of such indicators for SOH estimation at currents up to C/2. On the other hand, regarding peak tracking for the identification of degradation mechanisms, low currents are advisable, as errors up to 64 % were found and some indicators could not even be identified when charging C-rate increased.

The increase in temperature negatively affects the selected SOH indicator (voltage in valley 1) at advanced stages of aging. However, its maximum absolute error was found to be 1.5 %, so temperatures up to 45 °C could be considered for this purpose. On the other side, IC tracking for degradation assessment is much more affected by temperature, especially at low SOH. Thereby, it is not advisable to increase test temperature to this end.

All in all, this contribution highlights the potential of ICA as SOH estimation technique and identification tool for degradation mechanisms in SLB. The main reasons are the consistent evolution during second-life lifetime and the possibilities regarding test acceleration with higher current and temperature for SOH estimation. However, it is not recommended to accelerate IC testing to identify degradation mechanisms. Given the existing challenges in the repurposing process, ICA is a promising solution to characterize and assess degradation mechanisms in second-life batteries.

ACKNOWLEDGMENT

This work has been supported by the Spanish State Research Agency (AEI) under grants PID2019-111262RB-I00 /AEI/ 10.13039/501100011033 and DPI2016–80641-R, the European Union under the H2020 project STARDUST (774094), the Government of Navarra through research project 0011–1411–2018–000029 GERA and the Public University of Navarre under project ReBMS PJUPNA1904.

REFERENCES

[1] International Energy Agency, “Global EV Outlook 2021,” 2020. doi: 10.1787/d394399e-en.

[2] C. Curry, “Lithium-ion Battery Costs and Market, BNEF, 5 July 2017.” Bloomberg New Energy Finance, 2017, [Online]. Available: https://data.bloomberglp.com/bnef/sites/14/2017/07/BNEF-Lithium-ion-battery-costs-and-market.pdf.

[3] E. Braco, I. San Martín, A. Berrueta, P. Sanchis, and A. Ursúa, “Experimental Assessment of First- and Second-Life Electric Vehicle Batteries: Performance, Capacity Dispersion and Aging,” *IEEE Transactions on Industry Applications*, vol. 9994, no. 774094, 2021, doi: 10.1109/TIA.2021.3075180.

[4] Y. Zhang *et al.*, “Performance assessment of retired EV battery modules for echelon use,” *Energy*, vol. 193, p. 116555, 2020, doi: 10.1016/j.energy.2019.116555.

[5] E. Braco, I. San Martín, A. Berrueta, P. Sanchis, and A. Ursúa, “Experimental assessment of cycling ageing of lithium-ion second-life batteries from electric vehicles,” *Journal of Energy Storage*, vol. 32, no. July, p. 101695, 2020, doi: 10.1016/j.est.2020.101695.

[6] C. White, B. Thompson, and L. G. Swan, “Repurposed electric vehicle battery performance in second-life electricity grid frequency regulation service,” *Journal of Energy Storage*, vol. 28, no. January, p. 101278, 2020, doi: 10.1016/j.est.2020.101278.

[7] H. Li, M. Alsolami, S. Yang, Y. M. Alsmadi, and J. Wang, “Lifetime Test Design for Second-Use Electric Vehicle Batteries in Residential Applications,” *IEEE Transactions on Sustainable Energy*, vol. 8, no. 4, pp. 1736–1746, 2017, doi: 10.1109/TSTE.2017.2707565.

[8] T. Alharbi *et al.*, “Planning and Operation of Isolated Microgrids Based on Repurposed Electric Vehicle Batteries,” *IEEE Transactions on Sustainable Energy*, vol. 8, no. 7, pp. 41852–41859, 2019, doi: 10.1109/TII.2019.2895038.

[9] M. Dubarry *et al.*, “Identifying battery aging mechanisms in large format Li ion cells,” *Journal of Power Sources*, vol. 196, no. 7, pp. 3420–3425, 2011, doi: 10.1016/j.jpowsour.2010.07.029.

[10] D. Ansean *et al.*, “Lithium-Ion Battery Degradation Indicators Via Incremental Capacity Analysis,” *IEEE Transactions on Industry Applications*, vol. 55, no. 3, pp. 2992–3002, 2019, doi: 10.1109/TIA.2019.2891213.

[11] D. I. Stroe and E. Schaltz, “SOH Estimation of LMO/NMC-based Electric Vehicle Lithium-Ion Batteries Using the Incremental Capacity Analysis Technique,” *2018 IEEE Energy Conversion Congress and Exposition, ECCE 2018*, no. Ic, pp. 2720–2725, 2018, doi: 10.1109/ECCE.2018.8557998.

[12] E. Schaltz, D. I. Stroe, K. Norregaard, L. S. Ingvardsen, and A. Christensen, “Incremental Capacity Analysis Applied on Electric Vehicles for Battery State-of-Health Estimation,” *IEEE Transactions on Industry Applications*, vol. 57, no. 2, pp. 1810–1817, 2021, doi: 10.1109/TIA.2021.3052454.

[13] A. Fly and R. Chen, “Rate dependency of incremental capacity analysis (dQ/dV) as a diagnostic tool for lithium-ion batteries,” *Journal of Energy Storage*, vol. 29, no. February, p. 101329, 2020, doi: 10.1016/j.est.2020.101329.

[14] J. He, X. Bian, L. Liu, Z. Wei, and F. Yan, “Comparative study of curve determination methods for incremental capacity analysis and state of health estimation of lithium-ion battery,” *Journal of Energy Storage*, vol. 29, no. March, p. 101400, 2020, doi: 10.1016/j.est.2020.101400.

[15] H. Quinard, E. Redondo-Iglesias, S. Pelissier, and P. Venet, “Fast electrical characterizations of high-energy second life lithium-ion batteries for embedded and stationary applications,” *Batteries*, vol. 5, no. 1, 2019, doi: 10.3390/batteries5010033.

[16] Y. Jiang, J. Jiang, C. Zhang, W. Zhang, Y. Gao, and N. Li, “State of health estimation of second-life LiFePO4 batteries for energy storage applications,” *Journal of Cleaner Production*, vol. 205, pp. 754–762, 2018, doi: 10.1016/j.jclepro.2018.09.149.

[17] Z. Ma, Z. Wang, R. Xiong, and J. Jiang, “A mechanism identification model based state-of-health diagnosis of lithium-ion batteries for energy storage applications,” *Journal of Cleaner Production*, vol. 193, pp. 379–390, 2018, doi: 10.1016/j.jclepro.2018.05.074.

[18] Y. Dai, L. Cai, and R. E. White, "Capacity Fade Model for Spinel LiMn 2 O 4 Electrode," *Journal of The Electrochemical Society*, vol. 160, no. 1, pp. A182–A190, 2013, doi: 10.1149/2.026302jes.

[19] M. Lewerenz, A. Marongiu, A. Warnecke, and D. U. Sauer, "Differential voltage analysis as a tool for analyzing inhomogeneous aging: A case study for LiFePO4|Graphite cylindrical cells," *Journal of Power Sources*, vol. 368, pp. 57–67, 2017, doi: 10.1016/j.jpowsour.2017.09.059.